Mixing in a Cross-Flow-Impinging Jet Reactor

Patrice Nadeau, Dimitrios Berk, and Richard J. Munz
Dept. of Chemical Engineering, McGill University, Montreal, Canada

The mixing of a tracer in a reactor composed of two opposed jets perpendicular to a main stream is studied both experimentally and theoretically. For the experimental conditions, the gas flow was in a transitional state between laminar and turbulent due to the interaction of the mixed streams. Both the measurements and the mathematical model focus on the fluid flow (gas velocity) and the dispersion of a nonreacting species (tracer concentration) injected through one of the reactor streams. Two models are tested against experimental data: a laminar flow model (giving a time-dependent solution) and a standard k-ϵ turbulent flow model. These two models give quite different results, both qualitatively and quantitatively. This study demonstrates the importance of the selection of an appropriate mathematical model and computational domain.

Introduction

A lot of research has been conducted to produce ultrafine ceramic powders with particle sizes below 1000 nm. Some of the interest in ultrafine ceramic particles is due to the possibility of using lower sintering temperatures and improved properties of the material due to its finer microstructure (Pratsinis and Mastrangelo, 1989; Pratsinis et al., 1995). Although many processes can be used to synthesize these advanced ceramics, the use of aerosol reactors, that is, reactors that produce particles suspended in a gas, is advantageous because of their energy efficiency, the few steps involved compared to wet chemistry processes, and also their cleanliness.

A geometry that is often used for reactors producing ultrafine particles is that of a single or multiple jets discharging into a crossflow (Moura and Munz, 1997; Proulx and Bilodeau, 1991). Multiple jets are uniformly placed around the circumference of the tubular reactor, thus being opposed one relative to the others. In these reactors, the mixing, the cooling, the nucleation, and the growth of particles occur simultaneously. The reactors are often operated close to the transition between laminar and turbulent flow (especially for the jet flow, the crossflow being usually laminar before mixing), which causes irregular and unsteady flow patterns. This makes the mixing process quite complex and incompletely understood. Furthermore, the models are often tested with few experimental data (Soucy et al., 1994; Désilets et al., 1997), resulting in a limited assessment of the agreement between experimental and simulation data.

The articles of Chen and Hwang (1991) and Chang and Chen (1995) reported results for a geometry with some similarities to the one just discussed. However, their experimental conditions were quite different, with high Reynolds number hot jets discharging into a cold stream flowing in a narrow channel. Balabanova (1998) presents a study of the influence of mixing on the resulting aerosol particles using a one-dimensional model.

In this study, we characterize the mixing in a cross-flow-impinging jet reactor, both with experimental and modeling measurements. The jet Reynolds numbers correspond to transition flow conditions from laminar to turbulent ($100 \leq Re_j \leq 1{,}200$). The system considered is isothermal; the case of cold jets discharging into a hot stream is left for subsequent studies.

Experimental

Setup

The experimental reactor is shown in Figure 1 along with its main dimensions. Its overall shape is that of a rectangular duct. Compared to a cylindrical reactor, it has the advantage of liberating the side parallel to the x-axis from the jet. This face can then be used as a window for flow visualization and laser diagnostic techniques. Furthermore, the reactor has essentially a two-dimensional configuration. The reactor walls

Correspondence concerning this article should be addressed to R. J. Munz.

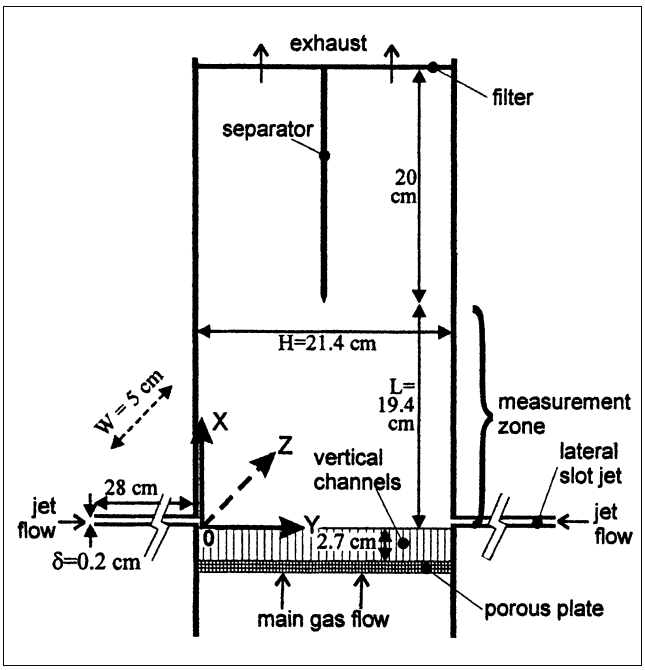

Figure 1. Cut view of the experimental reactor.

were made of acrylic polymer, except for two large quartz windows that covered the whole measurement zone in the *x-y* plane. Quartz was selected for its transparency extending to wavelengths of about 3.4 μm in the infrared light spectrum.

The main gas flow entered through the bottom of the reactor. It flowed upward through a high-pressure drop porous ceramic plate ($\Delta P \approx 10$ kPa) used to even the flow throughout the reactor cross-section. The main stream then passed in a series of vertical channels (a honeycomb) that straightened the flow. The secondary flow was separated into two equal flows prior to entering the reactor through the lateral slot jets. The two flows mixed primarily in the region denoted as the "measurement zone" of Figure 1. The gas flow moved upward in the reactor and exited through a glass-fiber filter. The left–right symmetry of the flow field was a major concern for this reactor. The use of the honeycomb, the separator, and the filter at the reactor exit helped in maintaining the symmetry.

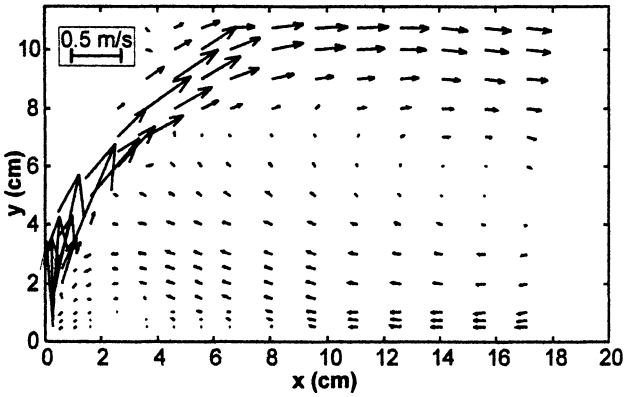

Figure 3. Measured velocity field for $V_j = 0.93$ m/s.

The gas used was nitrogen at ambient conditions ($T = 298$ K, $P = 1$ atm, $\rho = 1.12$ kg/m^3, and $\eta = 0.0000178$ Pa·s from Incropera and DeWitt, 1990). For concentration measurements, the tracer used was methane ($\rho = 0.643$ kg/m^3 and $\eta = 0.111 \cdot 10^{-4}$ Pa·s from Perry et al., 1984) because it is a good infrared absorber at a laser wavelength of 3.39 μm. The inlet main flow velocity (U_∞) was set constant at 0.032 m/s, while the mean inlet jet velocity (V_j) was varied from 0.42 m/s to 4.67 m/s. The corresponding values of the Reynolds numbers were 164 for Re_∞ (based on reactor hydraulic diameter) and 106–1,178 for Re_j (based on the hydraulic diameter).

Gas velocity

The velocity of the gas was measured by laser Doppler anemometry (LDA) in combination with oil smoke particles. Because the smoke could only be injected through the jet flow (the porous ceramic plate in the main flow would have caught all the particles), some flow areas in the reactor where the jet stream did not go at all could not be measured. This was significant only for the lowest jet velocities where the mixing between the two flows was poor. Each measurement was the average of 500 to 2,000 individual particle velocities

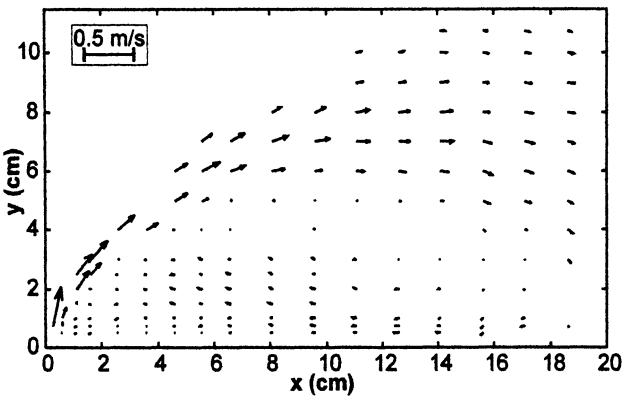

Figure 2. Measured velocity field for $V_j = 0.42$ m/s.

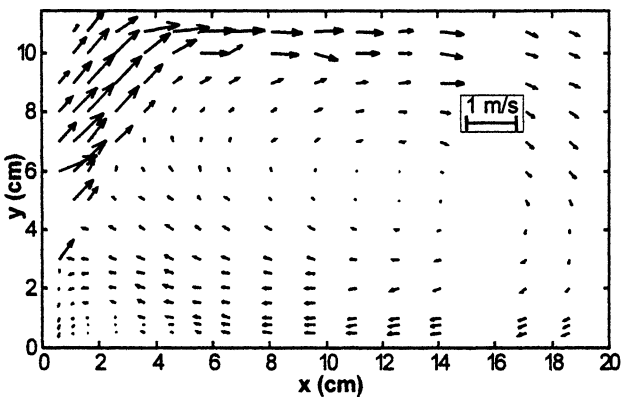

Figure 4. Measured velocity field for $V_j = 1.98$ m/s.

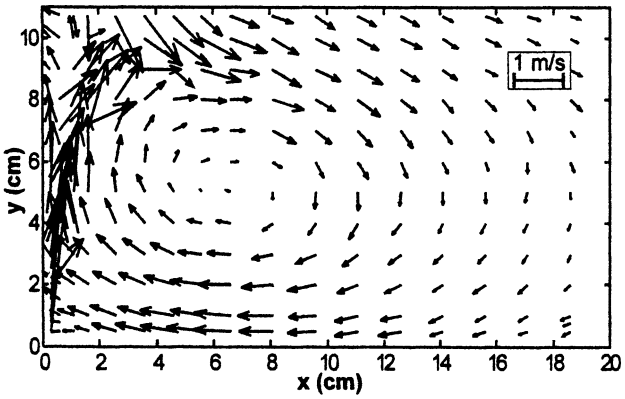

Figure 5. Measured velocity field for $V_j = 4.67$ m/s.

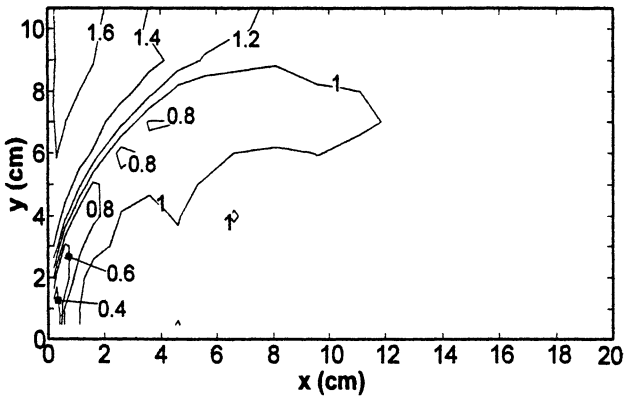

Figure 7. Measured tracer concentration field for $V_j =$ 0.93 m/s, tracer added to the main flow.

done over a 30- to 120-s period, depending on the local smoke concentration. From replicates, the uncertainty on the measurements (95% confidence intervals) was estimated at about $\pm 5\%$ in general, but it could go as high as $\pm 25\%$ in regions of high flow instabilities.

The measurements are displayed in Figures 2 to 5. Only one-half of the reactor ($0 \le y \le H/2$) is shown, since the other half is assumed to be symmetric (measurements confirming the validity of this assumption were done by Nadeau, 1999). All the figures show the same overall characteristics: a high-velocity jet that was deflected in the direction of the main flow, and a large recirculation zone along the wall. It appears that the main flow played a significant role in the bending of the jet only for the lowest two jet velocities. Since higher values resulted in a penetration to the half reactor width at very low x, this suggests that the opposed jets were primarily responsible for the jet deflection at $V_j \ge 1.98$ m/s.

It was difficult to conclude anything about the size of the recirculation zone as a function of V_j. Not only did the recirculation extend beyond the measurement zone, but its length was greatly influenced by the asymmetry in the flow. As can be observed for $V_j = 4.67$ m/s (Figure 5), the resultant from the impingement of the two jets was slanted slightly toward the lower y. This was probably caused by an imbalance in the two opposed jet flows. The consequence was a reduction in the length of the recirculation on the low y side. For the concentration measurements discussed below, smoke visualization experiments were used to correct by fine-tuning each jet flow the asymmetry observed in Figure 5.

Tracer concentration

The dispersion of an inert tracer inside the reactor gives a good estimate of the mixing between the main flow and the jets. Infrared (IR) laser absorption was used to measure the concentration of the tracer (methane) as a function of reactor location and inlet jet velocity. IR absorption spectroscopy is a widely used technique and will not be reviewed here; its application on-line in a reactor by using a laser beam was described in Nadeau et al. (1996). In order to avoid excessive inlet concentrations, methane was mixed with the main flow for lower V_j values and with the jet stream at higher velocities. The properties of the main gas (nitrogen) were not affected greatly by the tracer, since dilute concentrations were used. Each concentration measurement was an average of 2000 instantaneous readings sampled at a 1-kHz frequency.

In Figures 6–9, the mean tracer concentration inside the reactor is displayed for various jet velocities. The concentration (C) is normalized by the mixing-cup concentration (rang-

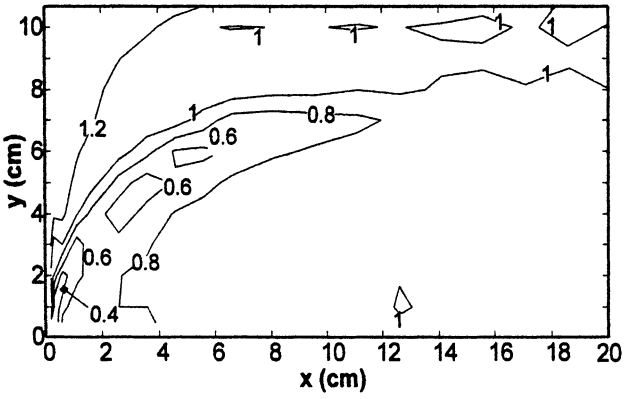

Figure 6. Measured tracer concentration field for $V_j =$ 0.42 m/s, tracer added to the main flow.

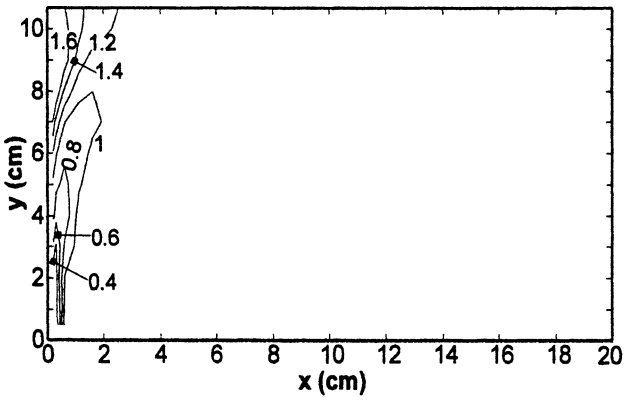

Figure 8. Measured tracer concentration field for $V_j =$ 1.98 m/s, tracer added to the main flow.

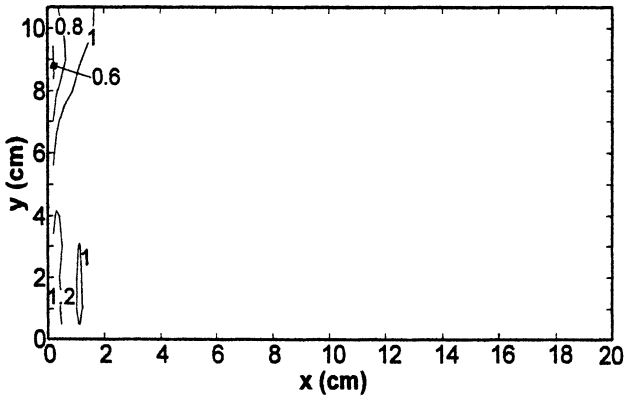

Figure 9. Measured tracer concentration field for V_j = 4.67 m/s, tracer added to the jet flow.

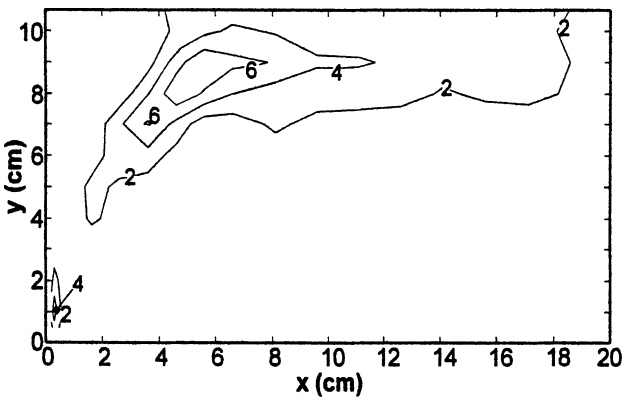

Figure 11. Measured concentration turbulence intensity field for V_j = 0.93 m/s (%).

ing from 6% to 7.3%, depending on the jet velocity), so that it is dimensionless with a value close to 1 corresponding to good mixing between the flows. The concentration range changed from one figure to another due to the variable inlet concentrations with jet velocity. The accuracy of the measurements was estimated from 95% statistical confidence intervals at about $\pm 4\%$.

For $V_j = 0.42$ m/s, the reactor portion corresponding to the main recirculation was at a lower concentration than the mixing cup. This suggests that the main flow did not incorporate itself well with the jet stream. This is also confirmed by the large area with $C \leq 0.8$ that followed the jet trajectory. For all higher jet velocities investigated, the tracer was at a concentration equal to the mixing cup in almost the whole recirculation zone. This can be explained by the improved mixing: the main flow completely penetrated the jet core to eventually mix with the recirculation by the swirls/eddies. For $V_j \geq 1.98$ m/s, almost the whole reactor was at a mean concentration equal to the mixing cup; only the regions close to the two flow inlets showed values different than 1. This shows the rapidity of the mixing, suggesting that perfect mixing may well approximate this system.

The concentration turbulence intensity is defined as the standard deviation of the instantaneous tracer concentration (σ_C) divided by its mean value (C) at a given location and multiplied by 100 to give a percentage. The fluctuations can be explained by large swirls that entrain the largely undiluted main flow with the jet. The concentration turbulence intensity fields are shown in Figures 10 through 13, which correspond to the concentrations shown in Figures 6–9, respectively. The uncertainty of the individual data points was around $\pm 15\%$ based on 95% confidence intervals. The values in these plots give an idea of the level of micromixing present in the reactor (good micromixing corresponds to lower values in the plots). Only when $\sigma_C/C \cong 0$ and $C = 1$ is the flow well mixed at all scales. The values reported are valid to compare the mixing quality between different jet velocities and locations. However, the measurements were integrated over the reactor thickness, meaning that they overestimated the absolute quality of the mixing (see Nadeau et al., 1996).

For a jet velocity of 0.42 m/s, large values of σ_C/C started to appear only a certain distance downstream from the jet entrance. This suggests that only weak flow disturbances were originally produced and that they took a certain time to grow into large flow structures that incorporated the two streams. This observation is consistent with the one of Koller-Milojevic and Schneider (1993) for double concentric jets at similar Reynolds numbers. As V_j was increased, larger turbu-

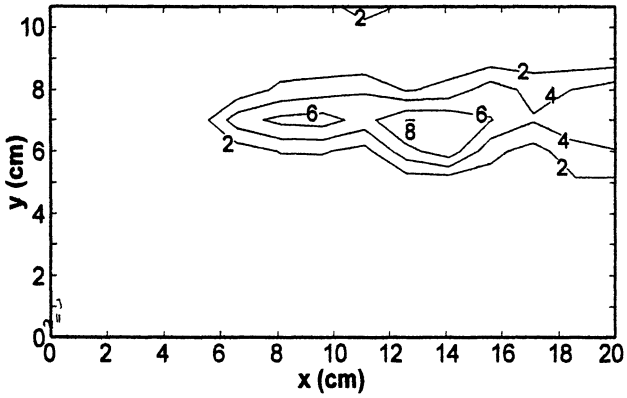

Figure 10. Measured concentration turbulence intensity field for V_j = 0.42 m/s (%).

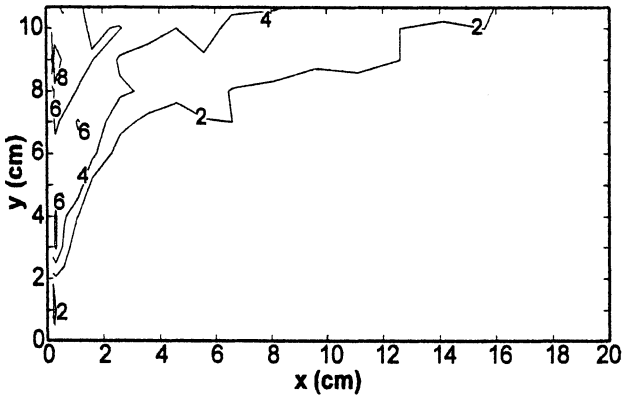

Figure 12. Measured concentration turbulence intensity field for V_j = 1.98 m/s (%).

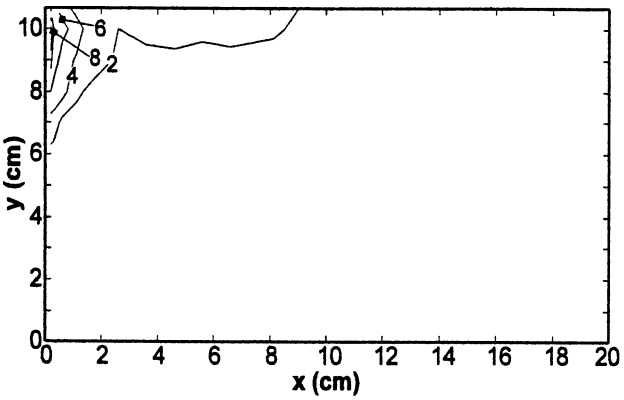

Figure 13. Measured concentration turbulence intensity field for $V_j = 4.67$ m/s (%).

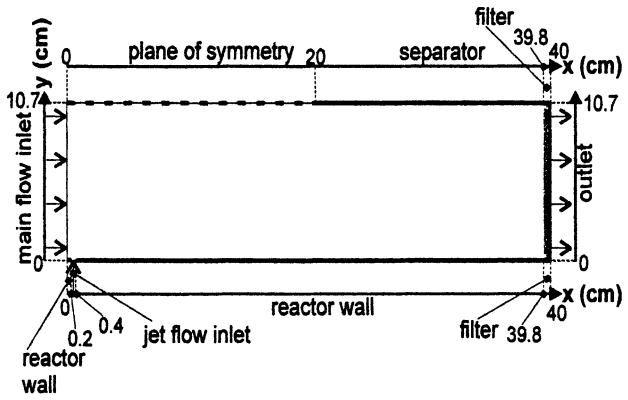

Figure 14. Computational domain.

lence intensities were found at lower x positions where the two opposing jets collided on each other and entrained the main flow. Also, the area of poor micromixing decreased from Figure 11 to 13, confirming that a better overall mixing was achieved with higher jet velocities. Figure 10 may appear to be an exception to this trend, but this is probably due to the poor micromixing area extending beyond the measurement zone.

Mathematical Model

Model description

The fluid flow and tracer dispersion were modeled by using a commercial computational fluid dynamics code (CFD2000, made by Adaptive Research). The equations solved by this code were standard continuity and momentum-balance equations along with mass-balance equations for each gas species. The detailed equations with their boundary and initial conditions can be found in Nadeau (1999). The simulations were performed for an isothermal and incompressible system, and the properties were those of nitrogen and methane (the tracer) at ambient conditions. Some assumptions were required in order to truncate the physical domain and thus reduce the computation time. The most important one is that the domain was assumed to be two-dimensional, so the variations along the reactor thickness (z-axis) were ignored. Another assumption is that only one-half of the reactor was included in the computational domain based on the left–right symmetry, that is, y ranged from 0 to $H/2$ only. Compared to a model that would take into account the whole reactor in three dimensions, the mixing model used here may suffer some inaccuracies.

The computational domain over which the modeling was performed is displayed in Figure 14. The domain was subdivided into 127 by 50 elements in the x- and y-directions, respectively, resulting in a total of 6350 elements. The solution was computed at 6528 nodes. The element size was variable so that the regions of steeper gradients contained a higher density of elements. Larger flow gradients were found close to the inlets and along the walls where the boundary layers developed. The dimensions of the computational domain were the same as the experimental reactor except for its length, which was longer by a few millimeters. This was not believed to significantly affect the flow field since it represented a difference of 2% only.

The various boundaries are also shown in the figure, along with their positions. The main flow inlet velocity was laminar, constant, and equal to U_∞. A fully developed laminar velocity profile between two flat plates was assumed for the jet inlet velocity. For the computations, both the reactor wall and separator were considered to be impermeable walls. The plane of symmetry was also impermeable, that is, there was no flux across it. The no-slip boundary condition for the velocity did not apply at the plane of symmetry. At the exit, a zero diffusion flux of momentum or mass was applied and the pressure was set equal to the value at ambient conditions. For the velocity simulations, a porous medium was simulated at the reactor outlet. This is not a boundary condition, but rather a volumetric flow constraint; it filled the last 2 mm along the x-axis of the domain. The purpose of this porous medium was to simulate the effect of the filter placed at the outlet of the experimental reactor. Its permeability was selected to cause a pressure drop equal to the one observed experimentally (of the order of 1 kPa). This pressure drop prevented reentering flow and flattened the velocity profile along the y-direction at the exit.

Gas velocity

Two flow models were used for the simulation: laminar and turbulent. The laminar solution was completed only for $V_j = 0.93$ m/s. The resulting flow field was time-dependent, but exhibited cycles (which is not so surprising considering that the jet Reynolds number falls within the transition zone)—a complete cycle took about 10 s. Five snapshots of the laminar velocity field are displayed in Figure 15; they show the typical flow patterns observed in a cycle. A "main" recirculation was always created directly downstream of the jet entrance, but its size was a function of time. This recirculation started with a small size and was located near the reactor wall. As time went on, it grew in size to eventually cover the full half-width of the reactor. The recirculation then extended in length until it separated into two recirculations: a larger one that was entrained downstream in the reactor, and a smaller one directly past the jet entrance. The smaller recirculation then became the new "main" recirculation, starting the next flow

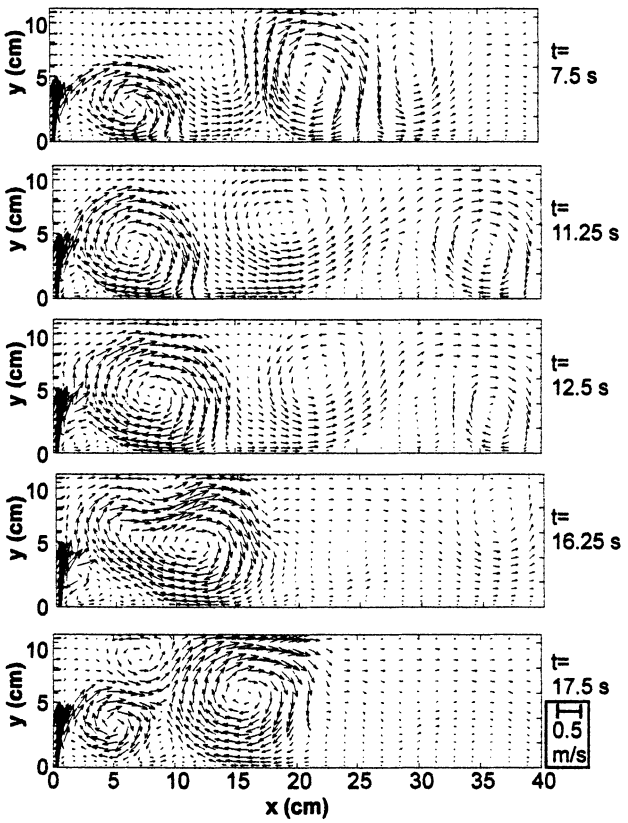

Figure 15. Laminar velocity field at various times: V_j = 0.93 m/s.

cycle. At least due to their instantaneous nature, the exact flow structures of Figure 15 were not observed experimentally. The laminar flow model nevertheless suggested a possible mechanism by which the flow can be time-dependent, as observed experimentally.

It is useful to average the laminar velocities over many flow cycles in order to compare the agreement of this model with experimental results. Figure 16 shows an average over a 40-s period (about four flow cycles). Comparing this figure with the measurements of Figure 3, the principal jet trajectory reached the reactor plane of symmetry ($y = H/2$) at $x \cong 6$ cm in both plots. A major flow recirculation was still observed past the jet entrance, but it did not extend as far downstream as was observed experimentally. Instead, the flow from the main jet trajectory was deviated toward the reactor wall past

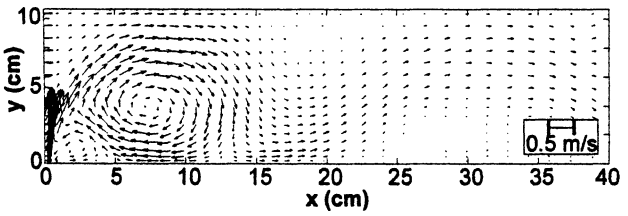

Figure 16. Mean laminar velocity field: V_j = 0.93 m/s, averaged over a 40-s period.

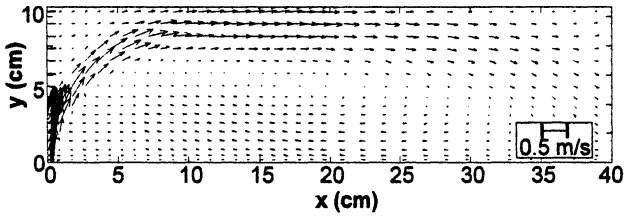

Figure 17. Turbulent velocity field: V_j = 0.93 m/s.

the recirculation (at about $x = 15$ cm), creating a secondary recirculation near the plane of symmetry (at about $x = 18$ cm).

Turbulent flow fields using a two-parameter k-ϵ model were computed for two values of V_j: 0.93 and 1.98 m/s. Because the instantaneous velocity fluctuations characteristic of turbulent flow are averaged over time by the k-ϵ model, only steady-state flow fields were computed. They are shown in Figures 17 and 18. The two flow fields had similar characteristics: a principal jet trajectory that reached the half-width of the reactor at low x-values, and one large recirculation that extended from the jet entrance to the reactor outlet filter. For the turbulent model at $V_j = 0.93$ m/s, the jet reached the reactor plane of symmetry at $x \cong 8$ cm, compared to $x \cong 6$ cm experimentally. Thus, in the model, the jet was deflected more by the main flow than in the experimental case. This was not observed at $V_j = 1.98$ m/s where both the model and measurements agreed well ($x \cong 1$ cm). One can explain this behavior by the transfer of momentum between the jet and the main flow. The experimental flows likely entered the reactor in a laminar state due to the porous plate and the long ducts prior to the jet entrances. At $V_j = 0.93$ m/s, it took a certain time (or distance) for the flow disturbances to grow to a large enough size so that turbulence became significant. Consequently, the momentum transfer between the two flows was initially poor, resulting in a jet that rapidly penetrated to the plane of symmetry. In the turbulent model, fully developed turbulence was assumed right at the entrance. This artificially improved the momentum transfer between the jet and main flow, resulting in a more deflected jet trajectory. At a jet velocity of 1.98 m/s, flow disturbances grew into turbulence faster, resulting in an experimental flow that approached the fully turbulent state very close to the inlets. The turbulent model then constituted a better approximation to the real flow. Compared to experimental observations (Figures 3 and 4), the laminar flow model underestimated the "main" recirculation length by 5–10 cm, while the turbulent model overestimated it for both values of V_j by 15–20 cm.

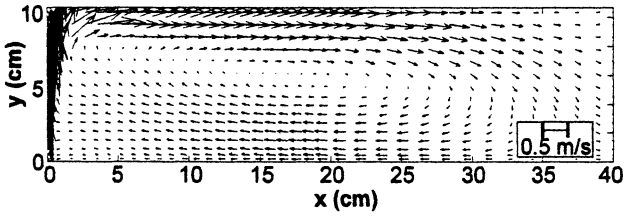

Figure 18. Turbulent velocity field: V_j = 1.98 m/s.

Table 1. Averaged Velocities (x Component) from Measurements and Mathematical Models

V_j (m/s)	U Along the Jet (m/s), $8 \le x \le 12$ cm, $9 \le y \le 10.7$ cm			U in the Recirculation (m/s), $4 \le x \le 8$ cm, $0 \le y \le 3$ cm		
	Exp.	Lam.	Turb.	Exp.	Lam.	Turb.
0.93	0.28	0.14	0.27	−0.064	−0.19	−0.044
1.98	0.44	—	0.64	−0.15	—	−0.088

Considering that the experimental flow was in a transition state from laminar to turbulent, the fluid mechanics models investigated appear as two limits in flow conditions.

So far, the discussion has been limited to the qualitative features of the flow fields. The values of the velocity vectors can also be compared to get a quantitative appreciation of the model agreement with experimental results. To do this, two representative positions were selected inside the reactor: one location corresponding to the main jet trajectory once it reached the half-width ($8 \le x \le 12$ cm, $9 \le y \le 10.7$ cm) and the other location in the recirculation close to the reactor wall ($4 \le x \le 8$ cm, $0 \le y \le 3$ cm). Several velocity vectors were averaged inside the prescribed limits and only the x-component of the velocity was considered. The values are listed in Table 1. At a jet velocity of 0.93 m/s, the laminar model disagreed with the experimental measurements, while the agreement of the turbulent model ranged from excellent (in the main jet trajectory) to fair (in the recirculation). At a jet velocity of 1.98 m/s, the agreement between the experiments and the turbulent model was only fair. This shows that even though some important features of the experimental flow were present in the simulation results, the numerical agreement between the two could still be improved. This could be achieved in future work by using a numerical simulation that would use the laminar flow equations, but would possibly take into account smaller scales of disturbances with a finer mesh. Alternatively, a turbulent model designed for low Reynolds numbers could also improve the solution.

Tracer concentration

The numerical simulation of the tracer dispersion served to evaluate the extent of the mixing between the two cross-streams. In Figure 19, the mean tracer concentration (again normalized by the reactor mixing-cup concentration) is displayed for the laminar flow model with $V_j = 0.93$ m/s. With the laminar flow model, the mixing was primarily due to alternating fluid layers of high and low concentrations that were entrained along the principal jet trajectory and the recirculation. The unsteady flow field stretched and dispersed these layers, which evened the tracer concentration. Both the experimental measurements and the mean tracer concentration from the mathematical model with laminar flow showed a similar mixing extent. The major difference was in the main recirculation where the model underpredicted the concentrations at $V_j = 0.93$ m/s by about 20%. The measurements suggested that the recirculation entrained fluid predominantly at high x-values, that is, when it was well mixed, since the concentration inside the recirculation was close to 1. In the model, a fraction of the early jet stream (containing no tracer) was transferred from time to time to the recirculation before it became well mixed with the main flow, thus giving a recirculation concentration less than 1.

The tracer concentration fields calculated from the turbulent flow model are given in Figures 20 and 21 for $V_j = 0.93$ and 1.98 m/s, respectively. For this model, the high eddy diffusion (calculated from the eddy viscosity assuming $Sc_t = 1$) and the expansion of the principal jet trajectory were primarily responsible for the dispersion of the tracer throughout the reactor. Overall, the trend was similar to that observed with the laminar flow model: the values along the jet trajectory were in good agreement with experiments, while those in the recirculation were lower. Here again, these lower concentrations were due to dilution of the recirculation from the early jet flow. As explained in the previous section, the experimental jet was initially laminar and turbulence grew to become significant only some distance downstream of the jet entrance. The k-ϵ model, with its assumption of fully developed turbulence right from the entrance, caused the jet flow to disperse quickly on each side of its main trajectory, thus diluting the tracer in the recirculation. This effect was less important for the higher jet velocity investigated. With increas-

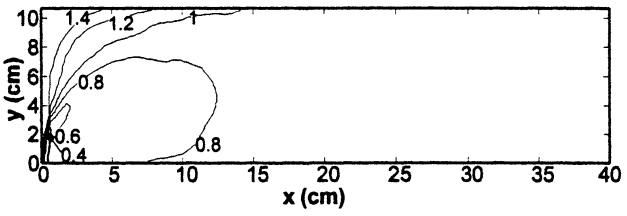

Figure 19. Tracer concentration field for $V_j = 0.93$ m/s with a laminar flow model, averaged over a 30-s period, tracer added to the main flow.

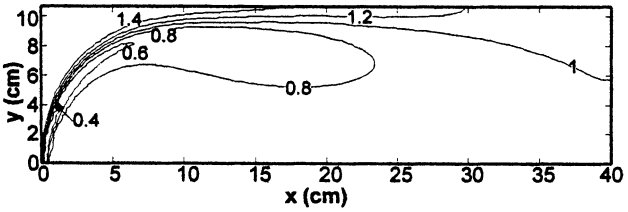

Figure 20. Tracer concentration field for $V_j = 0.93$ m/s with a turbulent flow model, tracer added to the main flow.

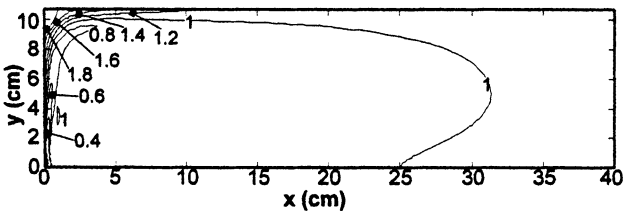

Figure 21. Tracer concentration field for $V_j = 1.98$ m/s with a turbulent flow model, tracer added to the main flow.

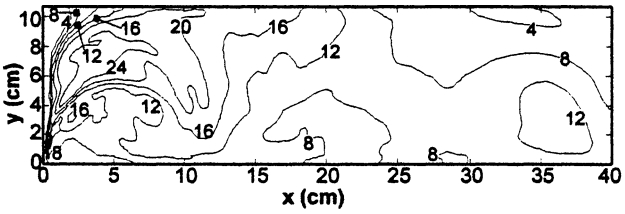

Figure 22. Tracer concentration turbulence intensity for $V_j = 0.93$ m/s with a laminar flow model.

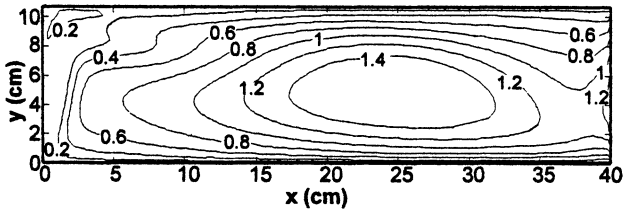

Figure 24. Tracer eddy diffusion coefficient for $V_j = 1.98$ m/s with a turbulent flow model ($m^2/s \cdot 10^3$).

ing jet velocity, the fluid along the principal jet trajectory reached the reactor mixing-cup concentration over a shorter distance. The fraction of the jet that mixed early with the recirculation thus had a higher tracer concentration, although still lower than 1.

The concentration turbulence intensities (σ_C/C) for the laminar flow model at a jet velocity of 0.93 m/s are plotted in Figure 22. An examination of this field reveals highly fluctuating tracer concentrations with peak values three times higher than their experimental equivalents. The fact that the measurements were integrated over the reactor thickness explains, at least in part, the higher computed values. For both the experimental and modeling results, the highest values were found in the jet core a few centimeters downstream from the jet inlet, which was the early region of intense mixing between the two streams. For the turbulent flow model, the tracer eddy diffusion coefficients (which are equivalent to the concentration turbulence intensities) are displayed in Figures 23 and 24. The higher their values, the higher the dispersion of tracer due to random instantaneous velocity fluctuations. Overall, the eddy diffusion coefficients ranged from one to two orders of magnitude higher than the molecular diffusion coefficient of methane ($D = 2.2 \cdot 10^{-5}$ m^2/s, from Reid et al., 1987). The peak values were about twice as high for $V_j = 1.98$ m/s than for $V_j = 0.93$ m/s, which is comparable to the increase in V_j between the two graphs. Also, the peaks occurred in the center of the recirculation, where the velocity vectors were close to zero. This indicated highly unstable velocities in this region, which were also observed experimentally. However, the measurements also showed high fluctuations near $y = H/2$, where the opposed jets contacted each other. The eddy viscosity from the model was quite low in this area, which contradicts the preceding experimental observation. It is believed that this inaccuracy was caused by the computational domain being truncated to one-half of the true reactor width, preventing the velocity at $y = H/2$ to fluctuate in the y-direction. This artificially reduced the contacting of the main flow with the jets.

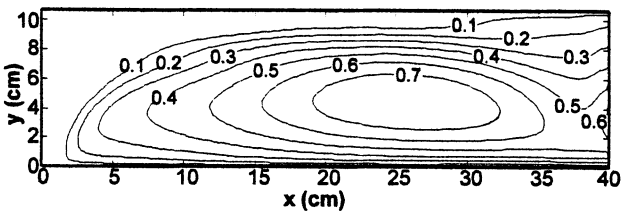

Figure 23. Tracer eddy diffusion coefficient for $V_j = 0.93$ m/s with a turbulent flow model ($m^2/s \cdot 10^3$).

Conclusions

This study focused on the measurement and modeling of the mixing in a cross-flow-impinging jet reactor. The flow was time-dependent due to the transition conditions, thus making the mixing between the streams a complex process. Higher jet velocities improved the quality of the mixing. The relatively uniform concentrations observed in the recirculation zone showed that little mixing occurred in that area. When modeling the fluid mechanics and the mass transfer, great care must be taken in the selection of the mathematical model and the computational domain, as they affect greatly the computed results. In fact, the use of different mathematical models and/or different computational domains (whole reactor/three-dimensional) could be the object of future work.

Acknowledgments

This research project was supported by the Government of Canada through the Natural Science and Engineering Research Council and by the Gouvernement du Québec through the Fonds pour la Formation des Chercheurs et l'Aide à la Recherche.

Notation

C = dimensionless mean tracer concentration at a given location
D = molecular diffusion coefficient, m^2/s
H = reactor width, m
L = length of the measurement zone, m
P = pressure, Pa
Re = Reynolds number
Sc_t = turbulent Schmidt number
T = temperature, K
U = x velocity component, m/s
V = y velocity component, m/s
W = reactor thickness, m
x = coordinate along the reactor length (origin at the honeycomb exit), m
y = coordinate along the reactor width (origin at the reactor wall), m

Greek letters

σ_C = standard deviation of the concentration at a given location
Δ = denotes a difference (like for a pressure drop)

Subscripts

j = jet
∞ = main flow

Literature Cited

Balabanova, E. G., "Rôle of the Mixing Process in a Flow Plasma Reactor for Ultrafine Powder Production," *High Temp.—High Pressures*, **30**, 493 (1998).

Chang, Y. R. and K. S. Chen, "Prediction of Opposing Turbulent Line Jets Discharged Laterally into a Confined Crossflow," *Int. J. Heat Mass Transfer*, **38**, 1693 (1995).
Chen, K. S., and J. Y. Hwang, "Experimental Study on the Mixing of One- and Dual-Line Heated Jets with a Cold Crossflow in a Confined Channel," *AIAA J.*, **29**, 353 (1991).
Désilets, M., J.-F. Bilodeau, and P. Proulx, "Modeling of the Reactive Synthesis of Ultra-Fine Powders in a Thermal Plasma Reactor," *J. Phys. D — Appl. Phys.*, **30**, 1951 (1997).
Incropera, F. P., and D. P DeWitt, *Introduction to Heat Transfer*, 2nd ed., Wiley, New York (1990).
Koller-Milojevic, D., and W. Schneider, "Free and Confined Jets at Low Reynolds Numbers," *Fluid Dyn. Res.*, **12**, 307 (1993).
Moura, F. J., and R. J. Munz, "Vapor-Phase Synthesis of Nanosize Aluminum Nitride Particles Using a Two-Stage Transferred Arc Reactor," *J. Amer. Ceram. Soc.*, **80**, 2425 (1997).
Nadeau, P., "Study of the Mixing with Chemical Reaction in a Cross Flow Impinging Jet Aerosol Reactor," PhD Thesis, McGill University, Montreal, P.Q., Canada (1999).
Nadeau, P., D. Berk, and R. J. Munz, "Non-Intrusive Fast Response Concentration Measurement Device for Chemical Reactors," *Rev. Sci. Instrum.*, **67**, 847 (1996).
Perry, R. H., D. W. Green, and J. O. Maloney, *Perry's Chemical Engineers' Handbook*, 6th ed., McGraw-Hill, New York (1984).
Pratsinis, S. E., and S. V. R. Mastrangelo, "Material Synthesis in Aerosol Reactors," *Chem. Eng. Prog.*, **85**, 62 (1989).
Pratsinis, S. E., G. Wang, S. Panda, T. Guiton, and A. W Weimer, "Aerosol Synthesis of AlN by Nitridation of Aluminum Vapor and Clusters," *J. Mat. Res.*, **10**, 512 (1995).
Proulx, P., and J.-F. Bilodeau, "A Model for Ultrafine Powder Production in a Plasma Reactor," *Plasma Chem. Plasma Process.*, **11**, 371 (1991).
Reid, R. C., J. M. Prausnitz, and B. E. Poling, *The Properties of Gases and Liquids*, 4th ed., McGraw-Hill, New York (1987).
Soucy, G., J. W. Jurewicz, and M. I. Boulos, "Mixing Study of the Induction Plasma Reactor: II. Radial Injection Mode," *Plasma Chem. Plasma Process.*, **14**, 59 (1994).

Manuscript received Jan. 19, 2000, and revision received Aug. 11, 2000.